Geophysical Journal International

Geophys. J. Int. (2010) **181,** 1395–1410 doi: 10.1111/j.1365-246X.2010.04592.x

Mineral magnetism to probe into the nature of palaeomagnetic signals of subtropical red soil sequences in southern China

Caicai Liu,[1,2] Chenglong Deng,[1] Qingsong Liu,[1] Longting Zheng,[3] Wei Wang,[4] Xinming Xu,[5] Sheng Huang[1,2] and Baoyin Yuan[1]

[1]*Paleomagnetism and Geochronology Laboratory (SKL-LE), Institute of Geology and Geophysics, Chinese Academy of Sciences, Beijing* 100029, *China. E-mail: cldeng@mail.iggcas.ac.cn*
[2]*Graduate School of the Chinese Academy of Sciences, Beijing* 100049, *China*
[3]*Anhui Museum, Hefei* 230061, *China*
[4]*Natural History Museum of Guangxi Zhuang Autonomous Region, Nanning* 530012, *China*
[5]*Zhejiang Province Institute of Cultural Relics, Hangzhou* 310014, *China*

Accepted 2010 March 8. Received 2010 March 5; in original form 2009 November 7

SUMMARY

Magnetic polarity stratigraphy has proved to be useful in dating of both marine and terrestrial sedimentary sequences over the world. However, the reliability of magnetostratigraphic results of red soil sequences in subtropical southern China has been found to be variable in different regions. To probe into the capabilities of recording magnetic polarity stratigraphy in the red soils, three red soil sequences have been selected for detailed mineral magnetic, petrographic and/or palaeomagnetic analyses. These include the Xuancheng and Qiliting sequences, which are located in the lower reaches of the Yangtze River and the Damei sequence in the Bose Basin near the Tropic of Cancer. Palaeomagnetic results indicate that the Xuancheng sequence has recorded the Brunhes Chron and the late Matuyama Chron, including a short interval probably representing the Santa Rosa geomagnetic event. The Xuancheng and Qiliting sequences have faithfully recorded the palaeogeomagnetic field behaviour while the Damei sequence has failed. Detailed mineral magnetic and petrographic measurements suggest that four magnetic minerals (magnetite, maghemite, haematite and goethite) are contained in the three studied sequences, but the characteristic remanent magnetization (ChRM) carriers are different. For the Xuancheng and Qiliting samples, the ChRM carriers are magnetite and haematite, which are all of detrital origin. However, the ChRMs of Damei samples are carried by pedogenic haematite with an unblocking temperature (T_B) of about 630–640 °C, which has overprinted the primary remanence of the Damei red soil deposits. This pedogenic haematite is mainly produced by chemical weathering, which is commonly intensified by the climate of high temperature and rainfall. It further suggests that climatic conditions have a great effect on the nature of palaeomagnetic signals of the red soil sequences. In addition, the red pigment components in the red soils may be used to indicate the degree of remagnetization.

Key words: Magnetic mineralogy and petrology; Magnetostratigraphy; Asia.

1 INTRODUCTION

The red soils studied are distributed to the south of the Qinling Mountains and the Huaihe River, which are the traditional dividing lines between temperate northern China and subtropical southern China (Fig. 1). They cover an area of about 2×10^6 km^2 in southern China (Yuan *et al.* 2008). As the most widely distributed Quaternary deposits in China, they contain a wealth of information on palaeoclimate, palaeoenvironment, geochronology and hominin evolution information (see reviews by Potts 2001; Yuan *et al*. 2008). Since the 1930s, these deposits have attracted more and more attention from palaeoclimatologists, geologists, geochronologists and palaeoanthropologists (Teilhard de Chardin *et al*. 1935; Yong *et al*. 1938; Xi 1991; Zhao & Yang 1995; Hou *et al*. 2000; Xiong *et al*. 2002; Qiao *et al*. 2003; Yin & Guo 2006; Deng *et al*. 2007; Lu 2000, 2007; Lu *et al.* 2008; Liu *et al*. 2008; Yuan *et al*. 2008). Recently, more Paleolithic sites have been discovered in the red soils (e.g. Fang *et al.* 1997; Hou *et al.* 2000; Xu *et al.* 2007; Liu *et al*. 2008; Wang *et al*. 2008). Especially, the Acheulean-like handaxes that were discovered and excavated from red soil sequences in the Bose Basin (Hou *et al.* 2000; Potts 2001; Wang *et al*. 2008) are of exceptional significance for understanding early hominin behavioural patterns (Hou

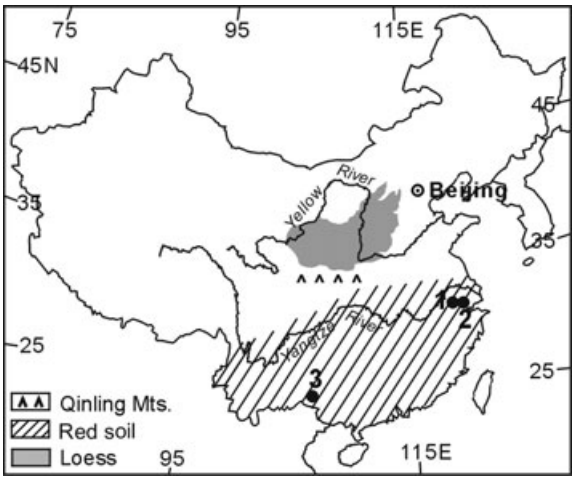

Figure 1. Schematic map showing the distribution of red soils in southern China and loess in northern China and the sections investigated in this study (after Liu *et al*. 2008). The Yellow River and Yangtze River are the major river systems in north and south China, respectively. The east–west trending Qinling Mountains are the traditional dividing line between temperate northern China and subtropical southern China. 1, Xuancheng; 2, Qiliting and 3, Damei.

et al. 2000; Potts 2001; Wang *et al*. 2008). Therefore, the dating of the red soil sequences has become increasingly crucial. However, because of the climatic conditions of high precipitation and warm temperature, which reduce the preservation of mammalian fossils and other dating materials, it is difficult to obtain detailed stratigraphic ages in the red soil area.

A series of magnetostratigraphic studies reveals that some sequences can record reliable geomagnetic polarities whereas others fail. For example, the red soil sequences in the middle–lower reaches of the Yangtze River have recorded magnetic polarity stratigraphies (Jiang *et al.* 1997; Qiao *et al.* 2003; Zhao *et al.* 2007; Liu *et al.* 2008), whereas the sequences near the Tropic of Cancer failed to record reliable palaeomagnetic field reversals (Deng *et al.* 2007; Yang *et al.* 2008) as the primary natural remanent magnetization (NRM) has been seriously overprinted by secondary chemical remanent magnetization (CRM) (Deng *et al.* 2007). Liu *et al.* (2008) suggested that the complicated palaeomagnetic behaviour of the red soil sequences may result from climatic differences, which control the intensity of chemical weathering. However, little is known about the exact nature of this overprinting.

In recent years, we have carried out systematic palaeomagnetic and mineral magnetic investigations on red soil sequences from different climate regimes and of different origins, such as those at Xuancheng and Qiliting, located along the lower reaches of the Yangtze River, and that at Damei, in the Bose Basin near the Tropic of Cancer. The Xuancheng sequence is of aeolian origin (Qiao *et al.* 2003), and the Qiliting and Damei sequences are of fluvial origin (Deng *et al.* 2007; Liu *et al.* 2008). Detailed palaeomagnetic investigations of the Qiliting and Damei sections have been addressed in our previous papers (Deng *et al.* 2007; Liu *et al.* 2008). In this study, we have conducted a palaeomagnetic investigation on the Xuancheng section and detailed mineral magnetic studies on the Xuancheng, Qiliting and Damei sequences to better understand the CRM acquisition process and its effects on the capabilities of recording magnetic polarity stratigraphy in Chinese red soil sequences.

2 SETTING AND SAMPLING

The Xuancheng red soil sequence (30°52.406′N, 118°51.899′E) (Fig. 1) has formed on terrace T2 of the Shuiyangjiang River, a tributary of the lower reaches of the Yangtze River. The Xuancheng area experiences a subtropical monsoon climate with a mean annual temperature (MAT) of 15−16 °C and a mean annual precipitation (MAP) of 1122–1400 mm (Qiao *et al.* 2003). The sequence includes three main pedostratigraphical units from top to bottom: (1) the Xiashu Loess with surface soil (0.7 m), loess (0.7–1.2 m) and palaeosol (1.2–1.7 m); (2) vermiculated red silty clay (1.7–10 m); (3) conglomerate (10 m to the bottom) with a maximum thickness in some sites up to 8 m. The upper two units are of aeolian origin (Xiong *et al.* 2002). A total of 95 block samples oriented by magnetic compass in the field were collected at 10 cm intervals from the depth interval of 0.6–10.4 m. These were later cut into cubic specimens of 2 cm edge length in the laboratory. The unheated left-overs of those samples were used for mineral magnetic and petrographic analyses.

The Qiliting red soil sequence (30°54.990′N, 119°41.112′E) (Fig. 1) has formed on terrace T2 of the Xitiaoxi River, a tributary of the Taihu Lake in the lower reaches of the Yangtze River. The MAT of this site is ∼16 °C and the MAP is ∼1300 mm with about 75 per cent of the precipitation falling from March to September (Liu *et al.* 2008). The Qiliting red soil sequence is of fluvial origin and is mainly composed of red clay and silts. The sequence, which is overlain by the Xiashu Loess Formation of aeolian origin and underlain by Cretaceous sandstone, can be subdivided into three lithological units from top to bottom: (1) the Xiashu Loess (0–1.5 m), (2) red clay and silts with vermiculated features (1.5–8.2 m) and (3) red sandy silts (8.2–11.2 m) (see Fig. 9 of Liu *et al.* 2008). Conglomerate clasts 2–5 mm in diameter sparsely occur in the sediments below 4.5 m depth. The sediments below 11.2 m depth were inaccessible due to road construction. Oriented palaeomagnetic samples were collected at 10 cm intervals from the depth interval of 1.5–11.2 m (Liu *et al.* 2008). In this study, the unheated left-overs of those palaeomagnetic samples were used for mineral magnetic and petrographic analyses.

The Damei red soil sequence (23°46.664′N, 106°43.720′E) (Fig. 1) has formed on terrace T4 of the Youjiang River in the Bose Basin (Hou *et al*. 2000; Potts *et al*. 2000), a NW to SE trending, elongated basin in the northwestern part of the Guangxi Zhuang Autonomous Region. The section is located near the Tropic of Cancer, where the climate is much hotter with a MAT of ∼22 °C and has alternating dry and wet seasons with more than 80 per cent of the precipitation usually falling in June, July and August, and a MAP of ∼1100 mm (Deng *et al.* 2007). This Damei sequence, which is of fluvial origin and underlain by Eocene sandstone (Wang *et al*. 2008), can be subdivided into six pedostratigraphical units from top to bottom (Deng *et al.* 2007): (1) cultivated soil, grey sandy-clay (0–0.1 m); (2) reddish-brown clay (0.1–0.8 m); (3) red clay with few vermiculated features (0.8–1.1 m); (4) vermiculated red clay (1.1–5.25 m); (5) red clay (5.25–8.35 m) and (6) well-sorted cobble conglomerate (8.35–12.35 m). Samples were collected from the depth interval of 0.1–8.35 m. Oriented palaeomagnetic block samples 10–20 cm in length were continuously taken in the field. Cubic specimens of 2 cm edge length with 2–4 cm intervals were cut from those block samples in the laboratory (Deng *et al.* 2007). In this study, the unheated left-overs of those palaeomagnetic specimens were used for mineral magnetic and petrographic analyses.

3 METHODS

3.1 Palaeomagnetic measurements

Palaeomagnetic measurements were carried out using a 2G Enterprises Model 760-R cryogenic magnetometer in a magnetically shielded space with residual fields smaller than 300 nT. All of the 95 oriented samples from the Xuancheng sequence were subjected to progressive thermal demagnetization (10–18 steps) up to a maximum temperature of 680 °C with 25–50 °C intervals below 585 and 10–15 °C above 585 °C, using a magnetic measurements thermal demagnetizer with a residual magnetic field less than 10 nT. Some sister samples were selected for progressive alternating field (AF) demagnetization at peak fields up to 100 mT at 2.5–10 mT intervals.

3.2 High-temperature magnetic measurements

High-temperature magnetic susceptibility measurements (χ–T curves) were made using a KLY-3 Kappabridge equipped with a CS-3 high-temperature furnace (Agico Ltd., Brno, Czech Republic). Each sample was heated from room temperature to 700 °C and then cooled back to room temperature in an argon atmosphere to minimize the possibility of oxidation. The average heating and cooling rates are approximately 12 °C min^{-1}. The sample holder and thermocouple contributions to magnetic susceptibility were subtracted.

High-temperature magnetization measurements (M_s–T curves) were performed in air using a magnetic measurements variable field translation balance by continuous exposure of samples through temperature cycles from room temperature to 700 °C and back to room temperature. The applied field strength was 500 mT.

3.3 Hysteresis properties

Samples were demagnetized in AFs up to 500 mT, and then were exposed to an applied field from 0 to 1.5 T to acquire isothermal remanent magnetizations (IRMs), using a MicroMag 2900 alternating gradient magnetometer (AGM) (Princeton Measurements Corp., NJ, USA). Subsequently, the saturation isothermal remanent magnetization (SIRM) (the IRM acquired at the maximum field of 1.5 T) was demagnetized in a stepwise direct current (DC) backfield to obtain the coercivity of remanence (B_{cr}) and the S ratio. S is defined as the absolute value of the IRM remaining after exposure to a reversed field of 0.3 T divided by the SIRM (King & Channell 1991; Verosub & Roberts 1995), namely, S ratio $= (-\mathrm{IRM}_{-0.3\mathrm{T}})/(\mathrm{SIRM}_{1.5\mathrm{T}})$. Hysteresis loops were also obtained using the MicroMag 2900 AGM. The magnetic field was cycled between $\pm$1.5 T. Coercivity (B_c) was determined after correcting for the paramagnetic contribution.

3.4 Thermal demagnetization of three-component IRM and $\mathrm{SIRM}_{2.7\mathrm{T}}$

Stepwise thermal demagnetization of the three orthogonal component IRM can be used to distinguish between magnetic minerals with different coercivities by their individual unblocking temperature. It is a powerful method to identify the ferrimagnetic mineral assemblage of a sample (Lowrie 1990; Verosub & Roberts 1995). Selected cubic samples from the three studied sequences were magnetized in successively smaller fields along three mutually orthogonal axes (Lowrie 1990), which are 2.7 T along the Z-axis (an appointed sample direction), 0.5 T along the Y-axis, 0.05 T along the X-axis, respectively (Zhu *et al.* 1994), to get a composite IRM, using a 2G Enterprises Pulse Magnetizer (2G660). These samples were then subjected to progressive thermal demagnetization (23 steps) up to 690 °C at 10–50 °C intervals. Accordingly, the IRM component of the X-axis represents the remanence carried by the low-coercivity or soft fraction, of the Y-axis, the medium-coercivity fraction, and of the Z-axis, the high-coercivity or hard fraction.

Another set of sister samples were first given a three-component IRM, and were then subjected to a 60 mT triaxial AF demagnetization followed by progressive thermal demagnetization as earlier.

The third set of cubic samples were magnetized in a field of 2.7 T only along the Z-axis of the sample to obtain SIRM (hereafter termed $\mathrm{SIRM}_{2.7\mathrm{T}}$), and then the $\mathrm{SIRM}_{2.7\mathrm{T}}$ was subjected to 100 mT AF demagnetization along the Z-axis, followed by progressive thermal demagnetization as earlier.

3.5 XRD analyses

X-ray diffraction (XRD) analyses were carried out using a DMAX2400 X-ray diffractometer to characterize the magnetic and clay mineral assemblages. The magnetic extracts were obtained by using a bar magnet with a field strength of >10 T.

4 RESULTS

4.1 High-temperature magnetic susceptibility (χ–T curves)

χ–T curves can help to identify the type of magnetic materials (Deng *et al.* 2001; Liu *et al.* 2005). The χ–T curves (Fig. 2) of the selected red soil samples from the three sequences all display a small hump near 300 °C. A decrease following this hump in the heating curves can be interpreted as the conversion of metastable ferrimagnetic maghemite to antiferromagnetic haematite (Deng *et al.* 2001; Liu *et al.* 2005). It is suggested that pedogenic fine-grained maghemite usually has a susceptibility drop between 300 and 400 °C (Liu *et al.* 2005). The marked decrease of magnetic susceptibility above 300 °C for selected samples from the Xuancheng and Qiliting sequences (Figs 2a–d) suggests that pedogenic maghemite may make significant contribution to the susceptibility of samples from these two sequences. A drop at about 585 °C on the heating curves of samples from the Xuancheng and Qiliting sequences (Figs 2a–d) suggests that magnetite is a contributor to magnetic susceptibility, especially for the Xuancheng samples (Figs 2a and b). For samples from the Qiliting sequence (Figs 2c and d), the large residual magnetic susceptibility above 585 °C becomes effectively zero at ~680 °C, the Néel temperature of haematite, which suggests that haematite is not only present but also in great amount due to its weakly magnetism. The same characteristic can also been seen in the high-temperature χ–T curves of some samples from the Xuancheng sequences, but to a lesser degree (e.g. Fig. 2b). This indicates that haematite with Néel temperature of 680 °C is also present but not abundant in samples from the Xuancheng section.

The χ–T curves of samples from the Damei sequence (Figs 2e and f) have obviously different features from the other two sequences, such as, a peak at about 510 °C on the heating curves, which may be caused by the neoformation of magnetite grains from

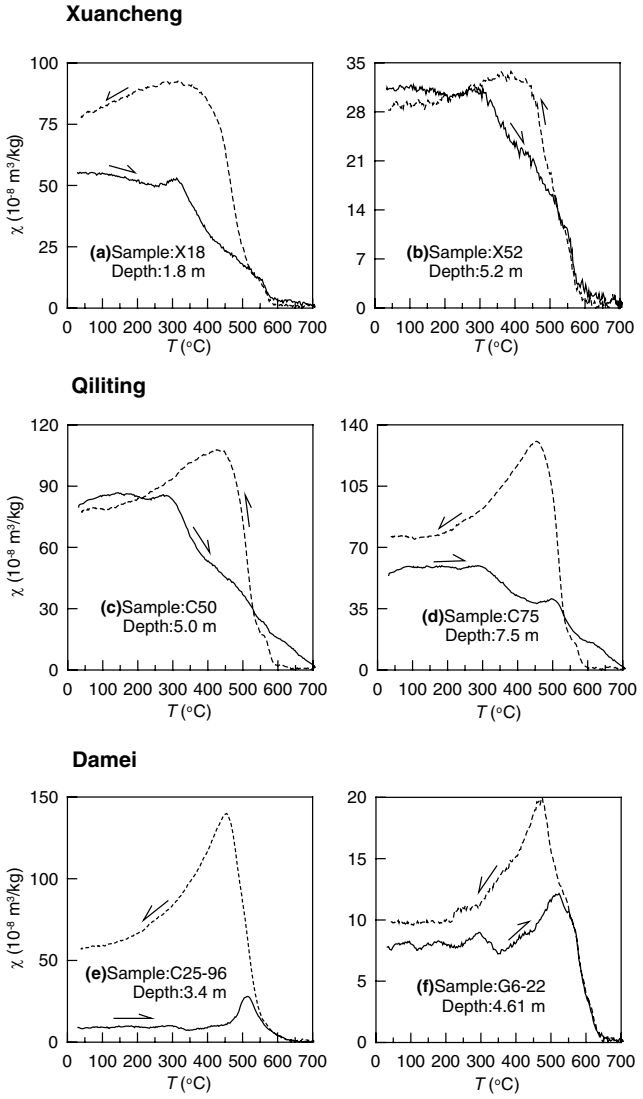

Figure 2. High-temperature magnetic susceptibility measurements (χ–T curves) of selected samples from the Xuancheng (a and b), Qiliting (c and d) and Damei (e and f) sections. Arrows as well as solid and dashed lines represent heating and cooling runs, respectively. χ–T data of the Qiliting section (c and d) are after Liu *et al*. (2008).

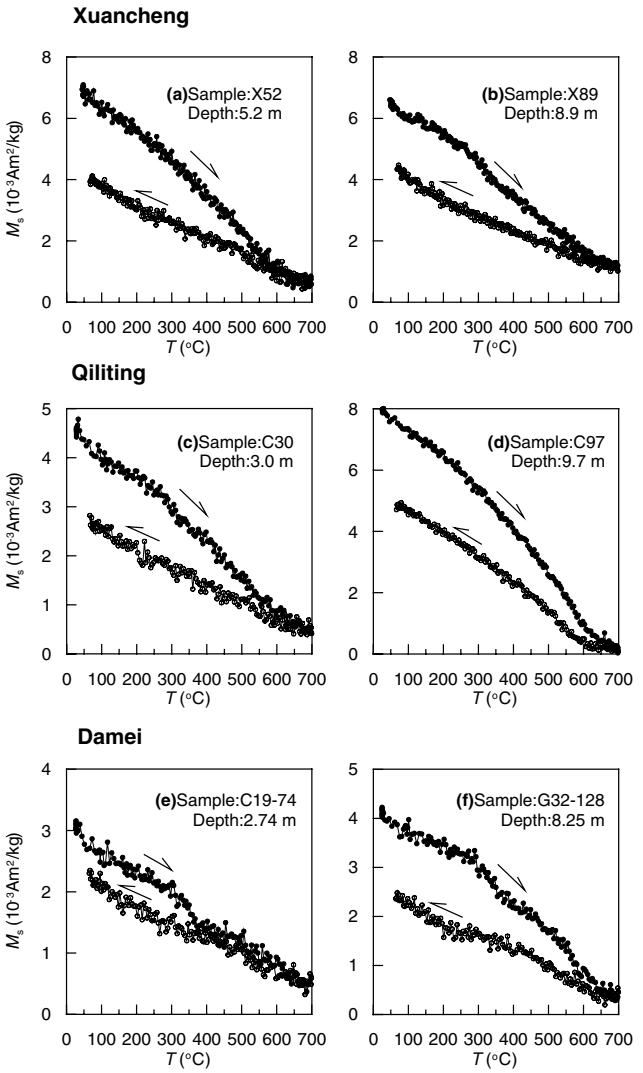

Figure 3. High-temperature magnetization (M_s–T curves) of selected samples from the Xuancheng (a and b), Qiliting (c and d) and Damei (e and f) sections. Solid and open circles represent heating and cooling runs, respectively. The applied field is 500 mT. M_s–T data of the Qiliting section (c and d) are after Liu *et al*. (2008).

iron-containing silicates/clays (Deng *et al.* 2001) or the reduction of haematite (Shive *et al.* 1977; Oches & Banerjee 1996).

All the cooling curves of the Xuancheng and Qiliting samples show a remarkable hump between 450 and 510 °C, some higher than the heating curves (e.g. Figs 2a,d and e), which may have resulted from the neoformation of fine-grained magnetite from iron-containing silicates/clays or the formation of magnetite by reduction of haematite (Hunt *et al.* 1995; Deng *et al.* 2001; Liu *et al.* 2005). For samples from the Damei sequence, the perfect reversibility above 550 °C suggests that the peak at about 510 °C results from the same phase (magnetite); as the peak on the cooling curve is clearly higher, indicating that much more magnetite has been formed above 550 °C. However, for samples from the Qiliting sequence, this reduction may be the main reason for the susceptibility loss between the heating and cooling curves above 585 °C (Figs 2c and d).

4.2 High-temperature magnetization (M_s–T curves)

M_s–T curves can provide useful information about magnetic mineralogy (Dunlop & Özdemir 1997). The M_s–T curves of selected samples from these three sequences are shown in Fig. 3. The conversion of metastable maghemite was not obvious on the M_s–T curves of samples from the Xuancheng and Qiliting sequences, except the curves of samples X89 and C30 (Figs 3b and c) which show a slight kink between 300 and 450 °C, whereas the M_s–T curves of samples from the Damei sequence display a notable conversion at about 350 °C (Figs 3e and f). This conversion of metastable maghemite to haematite (Stacey & Banerjee 1974) may result in the reduced magnetization intensity upon cooling. However, this reduction may also be caused by the oxidation of other magnetic minerals, such as magnetite, to haematite. All the heating curves show a steady decrease up to 680 °C, which further confirms the presence of haematite in samples from all these three sections. The presence of magnetite is displayed by the slight kink at about 585 °C in the M_s–T curves of

the Xuancheng and Qiliting samples (e.g. Figs 3a and d), but this is not distinct for the Damei samples.

4.3 IRM acquisition and DC field demagnetization of SIRM

IRM acquisition and DC field demagnetization of SIRM can provide information about the distribution of coercivity (B_c) and coercivity of remanence (B_{cr}), which can help to discriminate magnetic minerals with different B_c and B_{cr}. The wide range of the $IRM_{0.1T}$/SIRM and $IRM_{0.3T}$/SIRM values (Fig. 4) indicate a wide distribution of coercivity. Some samples from Xuancheng and Qiliting sections have a high $IRM_{0.1T}$/SIRM value close to 1 (Figs 4a and b), which suggests low-coercivity and ferrimagnetic mineralogy. However, the IRM of some samples (Fig. 4) continues to be acquired above 0.3 T, which is generally considered to be the theoretical maximum coercivity for magnetite grains. This indicates the abundant presence of high-coercivity magnetic minerals. In addition, some samples exhibit significantly low *S* ratios, which further confirms the presence of a high-coercivity magnetic phase, such as haematite and/or goethite. The *S* ratio values for some samples from the Damei sequence are much lower than the other two sequences, which suggests a higher concentration of high-coercivity magnetic minerals for the Damei samples. This is also confirmed by the relatively low $IRM_{0.1T}$/SIRM and $IRM_{0.3T}$/SIRM values for Damei samples compared with the samples from the other sequences.

4.4 Magnetic hysteresis

All of the selected samples, with the exception of sample X28, display pronounced wasp-waisted hysteresis loops (Fig. 5), which arise from the coexistence of two magnetic components with strongly contrasting coercivities (Roberts *et al.* 1995), such as the combination of low-coercivity magnetite and maghemite and high-coercivity haematite and goethite. Moreover, the wasp-waisted behaviour indicates a large concentration of hard components because they have weak magnetization (Roberts *et al.* 1995). The closed nature of the loop of sample X28 (Fig. 5a) below 0.3 T suggests that soft magnetic minerals control its hysteresis behaviour. In contrast, the open nature of the loop of sample G25-102 above 1.0 T (Fig. 5f) suggests the predominance of high-coercivity phases.

4.5 NRM demagnetization

The AF and thermal demagnetization curves of the NRM of the selected samples are shown in Fig. 6. The remanence intensities after a 100 mT AF demagnetization decrease to <40 per cent of the NRM for the Xuancheng samples (Fig. 6a), which demonstrates that the soft magnetic components carry a large part of the NRM; whereas the Damei samples have residual intensities of >40 per cent of the NRM (Fig. 6e), which indicates that hard magnetic minerals are the main carriers of the NRM. For the Qiliting sequences, some samples have residual intensities of <20 per cent of the NRM and some >40 per cent (Fig. 6c), which indicate that both soft and hard magnetic minerals contribute to the NRM. Thermal demagnetization of the NRMs of most selected samples displays broad distributions of unblocking temperatures. Some samples display a rapid decrease in remanence intensity below 200 °C, such as those at the depths of 0.9 and 2.8 m of the Xuancheng sequence (Fig. 6b), and that at 2.5 m depth in the Qiliting sequence (Fig. 6d), which may be due to the unblocking of goethite. In addition, some samples from the Xuancheng and Qiliting sequences (Figs 6b and d)

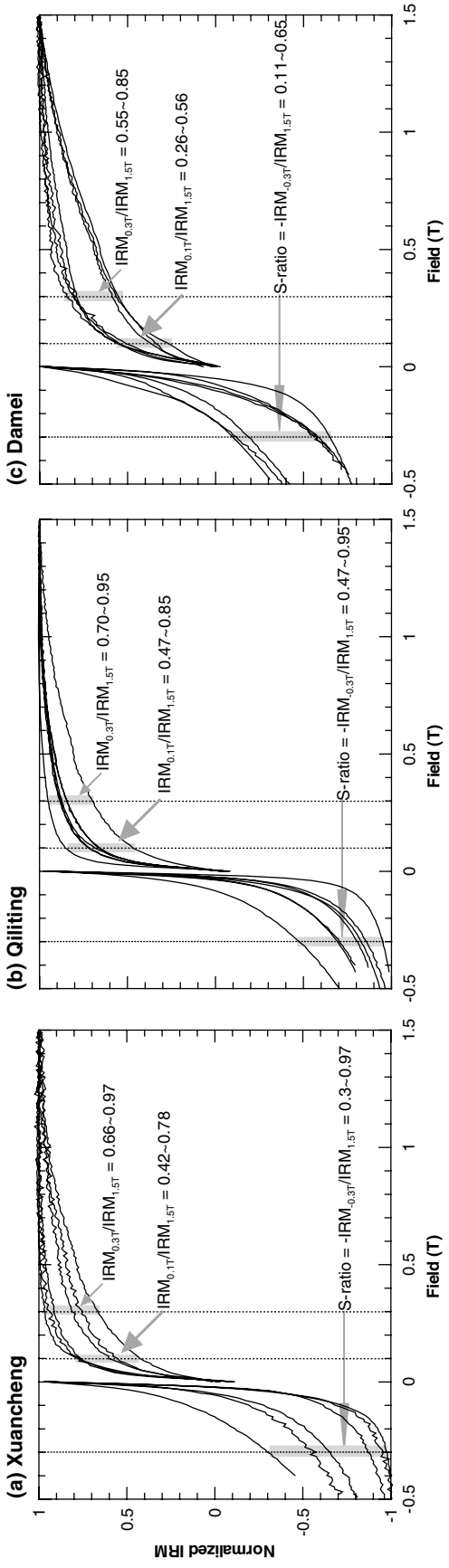

Figure 4. IRM acquisition curves and backfield curves of IRM of samples from (a) Xuancheng, (b) Qiliting and (c) Damei sections. The arrows indicate how $IRM_{0.1T}/IRM_{1.5T}$, $IRM_{0.3T}/IRM_{1.5T}$ and *S* ratio can be read directly from graph.

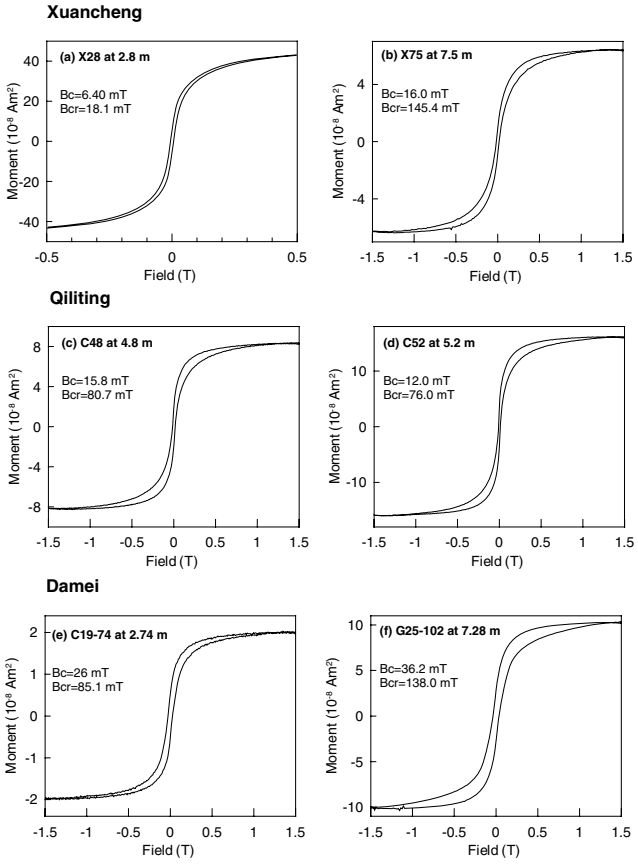

Figure 5. Hysteresis loops after slope correction for paramagnetic contribution. (a and b) Xuancheng samples, (c and d) Qiliting samples (after Liu *et al*. (2008)) and (e and f) Damei samples. For each sample, the hysteresis parameters were measured up to ±1.5 T. For clarity, the hysteresis loop of sample X28 (a) is cut-off at ±0.5 T.

have evident unblocking temperatures of 550–585 and 640–680 °C, suggesting that both magnetite and haematite are carriers of the NRM. Samples from the Damei sequence contain hard magnetic components such as haematite and goethite as suggested by XRD analyses (Deng *et al.* 2007) and by the AF demagnetization curves (Fig. 6e), whereas the thermal demagnetization curves do not show the unblocking temperature of goethite but show maximum temperatures of 500–585 °C, which look like the unblocking temperature of magnetite. However, the very low *S*-ratio values (Fig. 4) and a large residual NRM after AF demagnetization (Fig. 6e) suggest that soft magnetite is not the dominating mineral in Damei sequence. These maximum temperatures of 500–585 °C could be ascribed to the behaviour of high-coercivity pedogenic haematite. This pedogenic haematite may be fine-grained and Al-substituted (Herbillon & Nahon 1988; Liu *et al.* 2004), which may greatly decrease its unblocking temperature.

4.6 Thermal demagnetization of three-component IRM and $SIRM_{2.7T}$

Fig. 7 shows the thermal demagnetization curves of the three-component IRM and $SIRM_{2.7T}$ of selected samples from the Xuancheng sequence. A decrease in intensity at about 80 °C on the demagnetization curves of high- and medium-coercivity fractions (e.g. Figs 7a and c) is caused by the unblocking of goethite (Lowrie 1990). A slight slope change of the soft fraction curves at about 250–300 °C (e.g. Figs 7b–d) may be caused by the conversion of metastable maghemite, which may explain the large intensity decrease of the soft fraction. Another change in slope at about 585 °C suggests the presence of magnetite. The remanence intensities of all the three fractions decrease to zero up to about 680 °C (Figs 7a–d), the unblocking temperature of haematite or the conversion temperature of stable maghemite (Dunlop & Özdemir 1997). Comparing the thermal demagnetization curves of the two types of composite IRM, those that were not AF demagnetized (Figs 7a and b) and those that were subjected to 60 mT AF demagnetization (Figs 7c and d), respectively, we find that their behaviour is nearly the same except for the remanence intensity decrease of the soft fraction, which indicates that the magnetic phase with an unblocking temperature of about 680 °C (Fig. 7) is not soft maghemite but hard haematite. The haematite may have a wide grain size distribution, which causes the overlap of coercivity spectra. However, a large residual remanence intensity of the soft fraction after 60 mT AF demagnetization (e.g. Fig. 7d) suggests that the IRMs were not acquired in a perfectly orthogonal setup, which causes 'leakage' into the other IRM components. This effect should be limited and the thermal demagnetization analyses of the three-component IRM can still clearly discriminate other magnetic minerals (Figs 7a and b). The thermal demagnetization curves of the $SIRM_{2.7T}$ display conversions at about 120 °C (Fig. 7e) and 250–350 °C (Fig. 7f), and maximum unblocking temperatures of 680 °C (Figs 7e and g). This suggests that goethite, maghemite and haematite are the carriers of SIRM of the Xuancheng samples.

The thermal demagnetization curves of the three-component IRM and $SIRM_{2.7T}$ of the Qiliting samples (Fig. 8) show similar characteristics to those of the Xuancheng samples, such as a sharp decrease at 80−120 °C (Figs 8b–d), a change in slope at about 585 °C (Figs 8a–d) and a maximum unblocking temperature of 670–690 °C (Figs 8a–g). These characteristics suggest that the magnetic minerals of the Qiliting sequence consist of goethite, magnetite and haematite. Like the Xuancheng samples (Figs 7a–d), the Qiliting samples (Figs 8a–d) show similar characteristics between the thermal demagnetization curves of the composite IRMs that were not AF demagnetized (Figs 8c and d) and those that were subjected to 60 mT AF demagnetization (Figs 8c and d). The data indicate that haematite does not only control the high-temperature behaviour, but also constitutes a large proportion of the magnetic mineralogy, as suggested by the large residual remanence at high temperatures during thermal demagnetization of the $SIRM_{2.7T}$ (Figs 8e and g).

The thermal demagnetization curves of the three-component IRM of the Damei samples (Figs 9a–d) indicate different behaviours from the Xuancheng and Qiliting samples, except for the same inflection at about 80 °C on the curves of the high-coercivity fraction. A slight change in slope is evident at 585–610 °C on the demagnetization curves of the soft fraction for sample C19-73 (Fig. 9a), indicating the presence of small quantity of magnetite. The demagnetization curves of the soft fraction for sample G26-114 (Figs 9b and d) display two notable changes in slope at 120 and 250 °C, which can be respectively interpreted as the unblocking of goethite and the transformation of metastable pedogenic maghemite or titanomaghemite (Dunlop & Özdemir 1997). Considering the results of high-temperature magnetic susceptibility (Figs 2e and f) and magnetization (Figs 3e and f) analyses, this magnetic phase is more likely to be maghemite. The obvious remanence drop at 630–640 °C (e.g. Figs 9b and d) is interpreted as the unblocking of pedogenic haematite (Tauxe *et al.* 1980) or pure maghemite (Özdemir &

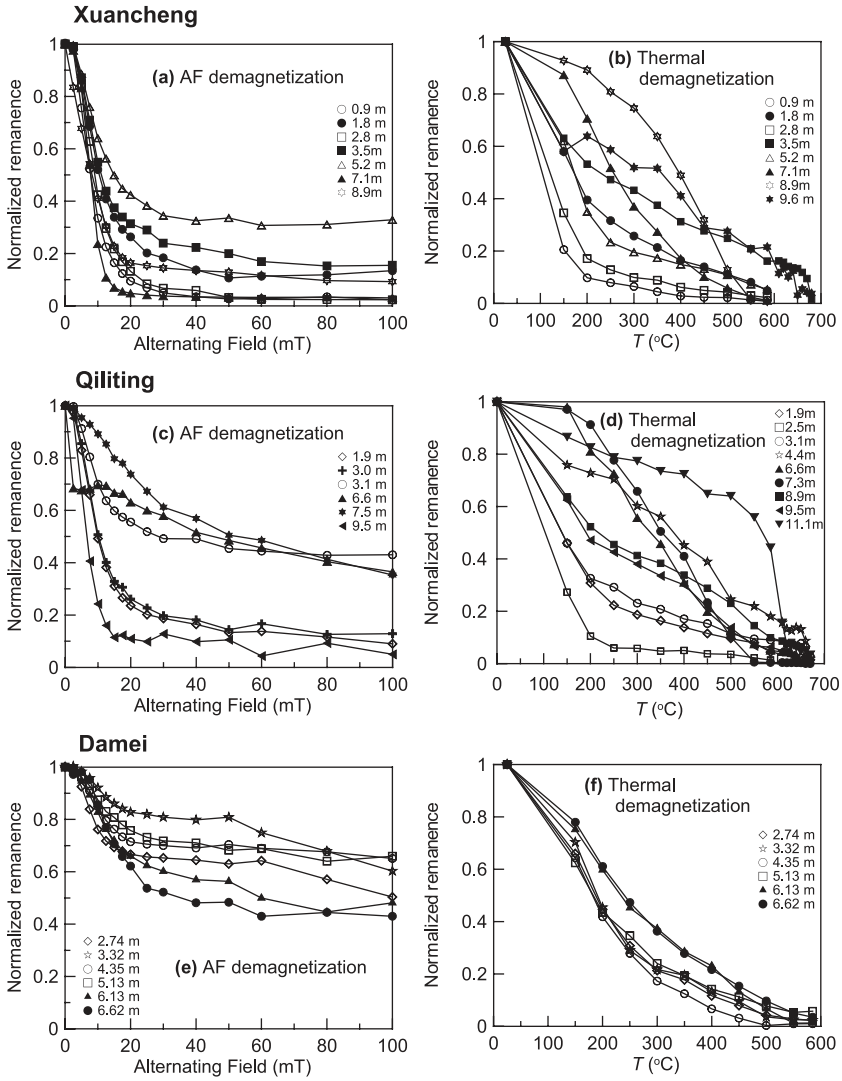

Figure 6. AF and thermal demagnetization curves of the NRM for selected samples from the Xuancheng (a and b), Qiliting (c and d) and Damei (e and f) sections. The left (a, c, e) and right (b, d, f) columns show AF and thermal demagnetization curves, respectively. Data shown in (d) are after Liu *et al*. (2008). Data shown in (e and f) are after Deng *et al*. (2007).

Banerjee 1984; Dunlop & Özdemir 1997). The high-temperature parts of the thermal demagnetization curves of the two types of composite IRMs, those that were not AF demagnetized (Figs 9a and b) and those that were subjected to 60 mT AF demagnetization (Figs 9c and d) have nearly the same characteristics, especially for sample G26-104 (Figs 9b and d). The data indicate that the unblocking of pedogenic haematite resulted in the remanence drop at 630–640 °C, not maghemite, because the remanence carried by maghemite can be easily removed by the 60 mT AF demagnetization due to its soft nature. Moreover, the unblocking temperature of 630–640 °C is most obvious in the high-coercivity fraction curves (Figs 9a and d), which indicates high-coercivity pedogenic haematite. In addition, the thermal demagnetization curves of $SIRM_{2.7T}$ of the Damei samples also display a sharp decrease to nearly zero at temperatures of 630–640 °C (Figs 9e–g), and little remanence remains above 640 °C, which suggests that the pedogenic haematite contributes significantly to the remanence and masks the signal of detrital haematite with Néel temperature of 680 °C. Besides pedogenic haematite, the two other main carriers of the SIRM of the Damei samples are goethite, as suggested by a marked decrease at about 80 °C (Fig. 9e), and maghemite, indicated by a conversion at about 250 °C (Fig. 9g).

The data of the Damei samples are obviously different from those of the Xuancheng and Qiliting samples. Magnetite, haematite, maghemite and goethite are all present in these three red soil sequences. However, the dominating magnetic minerals are different among these sequences. The main remanence carriers are pedogenic maghemite and detrital magnetite and haematite in the Xuancheng sequence, pedogenic maghemite and detrital haematite in the Qiliting sequence and pedogenic maghemite and haematite in the Damei sequence. Pedogenic magnetic minerals make a larger contribution to the remanence of the Damei samples than the other two sequences.

4.7 XRD analyses

XRD spectra of bulk samples and magnetic extracts from the studied three sections are shown in Fig. 10. The maximum peaks of the spectrum of each selected sample are all the characteristic peaks of

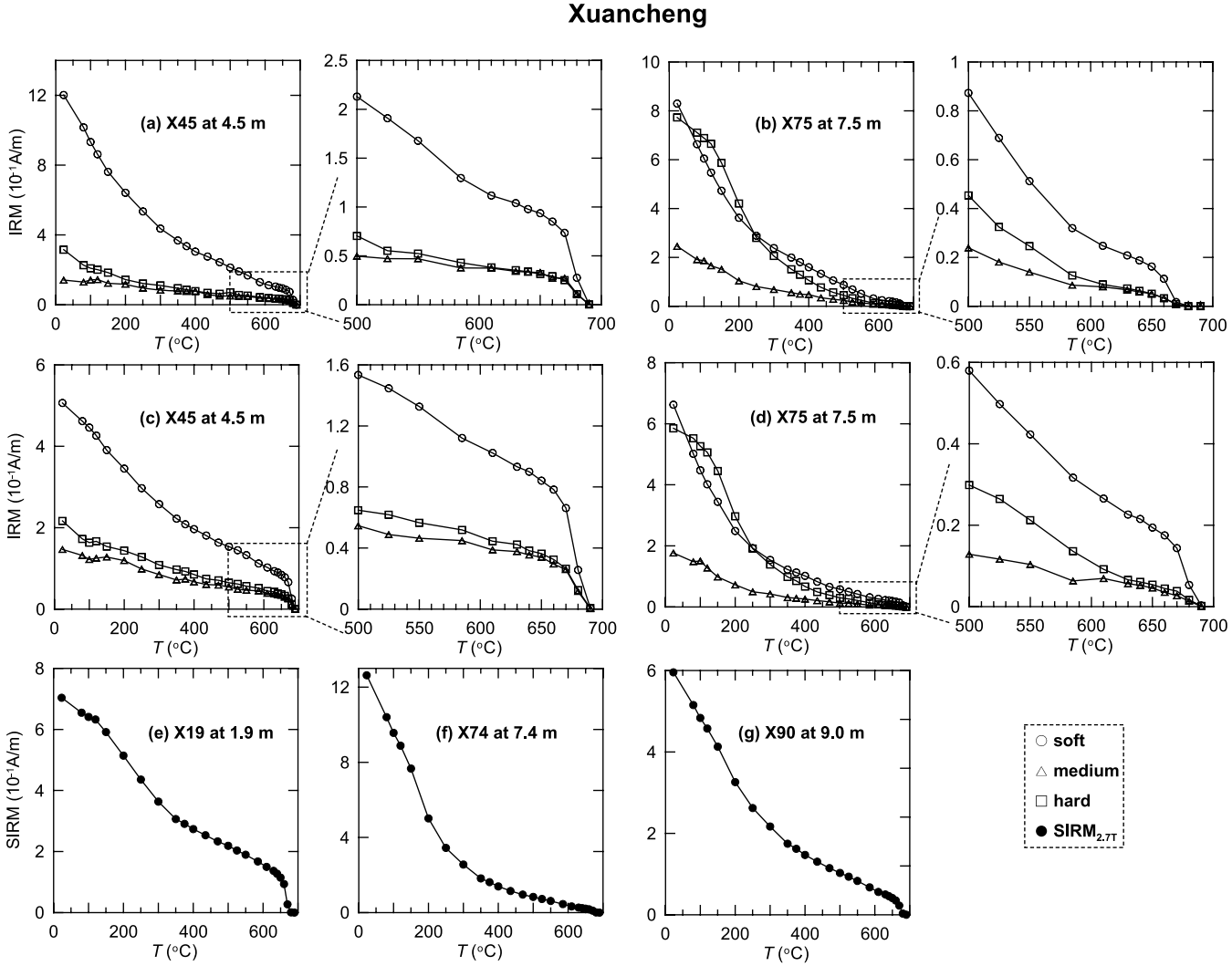

Figure 7. (a–b) Progressive thermal demagnetization of a three-component IRM (Lowrie 1990) produced by magnetizing samples from the Xuancheng section in 2.7, 0.5 and 0.05 T along the *Z*-, *Y*- and *X*-axes, respectively. (c–d) Progressive thermal demagnetization of a three-component IRM (Lowrie 1990), which is produced by magnetizing samples of the Xuancheng section in 2.7, 0.5 and 0.05 T along the *Z*-, *Y*- and *X*-axes, respectively, and then demagnetized in an alternating field of 60 mT along the *Z*-, *Y*- and *X*-axes. (e–g) Progressive thermal demagnetization of SIRM, which is produced by magnetizing samples of the Xuancheng section in 2.7 T along the *Z*-axis and then demagnetized in an alternating field of 100 mT also along the *Z*-axis.

quartz, which indicates that quartz dominates the coarse fraction of the red soils. All the selected samples contain illite and kaolinite as the main clay minerals, which are typical for tropical–subtropical soils (Yin & Guo 2006), but their concentrations are much higher in the Damei section, which possibly indicates much stronger chemical weathering because intense kaolinization occurs in the peak stage of weathering (Chen & Wang 2004). By comparing the spectra of bulk samples and magnetic extracts, we find that the characteristic peaks of haematite and maghemite become stronger after magnetic extraction for the Qiliting samples (Figs 10c and d). This behaviour is not obvious in the spectra of the Xuancheng and Damei samples (Figs 10a–b and e–f), but for the Damei samples, strong characteristic peaks of ilmenite appeared after magnetic extraction. This ilmenite should be of detrital origin and coarse-grained, which has a higher magnetization compared with pedogenic fine-grained antiferromagnetic minerals. Moreover, the pedogenic maghemite and haematite may form on the surface of the detrital ilmenite grains. Thus, this abundant present coarse-grained ilmenite can be easily extracted. In addition, the main characteristic peak of goethite is stronger for the Damei samples than for the Xuancheng and Qiliting samples, which suggests that a large portion of goethite may be contained in the Damei deposits.

4.8 Palaeomagnetic results

The intensity of the NRM of the samples from these three red soil sequences varies between 10^{-4} and 10^{-2} A m^{-1}. The principal component analyses were performed using the PaleoMag software developed by Craig H. Jones and Joya Tetreault. Progressive thermal demagnetization results were displayed by orthogonal diagrams (Zijderveld 1967) (Fig. 11). ChRM directions were computed by a least-squares fitting technique (Kirschvink 1980). For most samples from the Xuancheng and Qiliting sequences, the stable ChRM was resolved between 500 and 680 °C, after removing one or two soft, secondary components of magnetization (Figs 11b, c and e–i), which suggests that haematite is the main ChRM carrier. For some samples from the Xuancheng sequence, the ChRM components

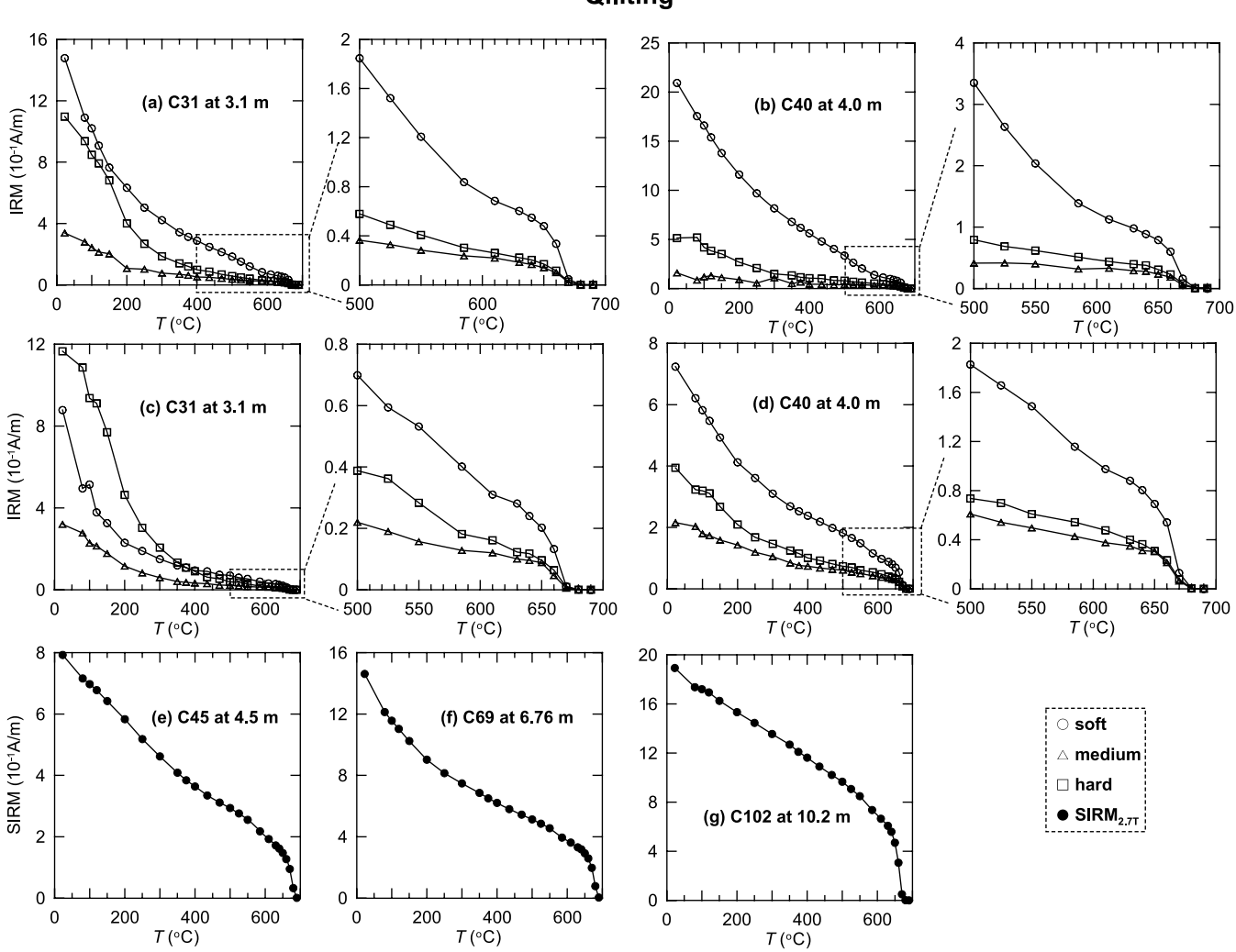

Figure 8. (a–b) Progressive thermal demagnetization of a three-component IRM (Lowrie 1990) produced by magnetizing samples from the Qiliting section in 2.7, 0.5 and 0.05 T along the *Z*-, *Y*- and *X*-axes, respectively. (c–d) Progressive thermal demagnetization of a three-component IRM (Lowrie 1990), which is produced by magnetizing samples of the Qiliting section in 2.7, 0.5 and 0.05 T along the *Z*-, *Y*- and *X*-axes, respectively, and then demagnetized in an alternating field of 60 mT along the *Z*-, *Y*- and *X*-axes. (e–g) Progressive thermal demagnetization of SIRM, which is produced by magnetizing samples of the Qiliting section in 2.7 T along the *Z*-axis and then demagnetized in an alternating field of 100 mT also along the *Z*-axis.

were defined between 300 and 585 °C (Figs 11a and d), which suggests that magnetite is the ChRM carrier. In most red soil sequences, the formation of pedogenic magnetic minerals often causes complicated palaeomagnetic behaviours (e.g. Figs 11b, e, f and i). The intensity of remanent magnetization of samples from the Damei sequence decreased to effective zero up to 585 °C, and the demagnetization curves of orthogonal vector for Damei samples are nearly linear (Figs 11j, k and l). These linear demagnetization curves may indicate chemical remagnetization after deposition.

In the Xuancheng sequence, 40 samples gave reliable ChRM directions. The maximum angular deviations (MAD) are smaller than 15°. Virtual geomagnetic pole (VGP) latitudes were calculated from the ChRM vector directions, which were subsequently used to define the succession of magnetostratigraphic polarity of the Xuancheng section (Fig. 12).

Two magnetozones were recorded in the Xuancheng sequence (Fig. 12f): one with normal polarity, N1 (0.6–6.55 m) and the other with reverse polarity, R1 (6.55 m to the bottom). Previous magnetostratigraphic studies of the red soil sequences in the middle–lower reaches of the Yangtze River have suggested that the sequences were deposited from the late Early to Middle Pleistocene (Jiang *et al.* 1997; Qiao *et al.* 2003; Zhao *et al.* 2007; Liu *et al.* 2008). The Xuancheng red soil sequence located in the lower reaches of the Yangtze River belongs to this geochronological framework. By correlating to the geomagnetic polarity timescale (Cande & Kent 1995; Opdyke & Channell 1996; Singer *et al*. 1999, 2002; Lourens *et al.* 2004), the normal magnetozone N1 recorded in the Xuancheng sequence corresponds to the Brunhes chron and the reverse magnetozone R1 to the late Matuyama chron. A short interval e1 (7.15–7.55 m) (Fig. 12f) may be interpreted as the Matuyama-Brunhes precursory excursion or the Kamikatsura geomagnetic event, both of which have been recorded in volcanic rocks or sediments (Hart & Tauxe 1996; Singer *et al.* 1999, 2002; Coe *et al.* 2004; Laj & Channell 2007), or the Santa Rosa geomagnetic event, which has also been observed in marine sediments (Channell *et al.* 2002; Horng *et al.* 2003; Laj & Channell 2007) and probably in terrestrial sediments (Wang *et al.* 2005; Deng *et al.* 2006; Liu *et al.* 2008). This short interval may more likely represent the Santa Rosa

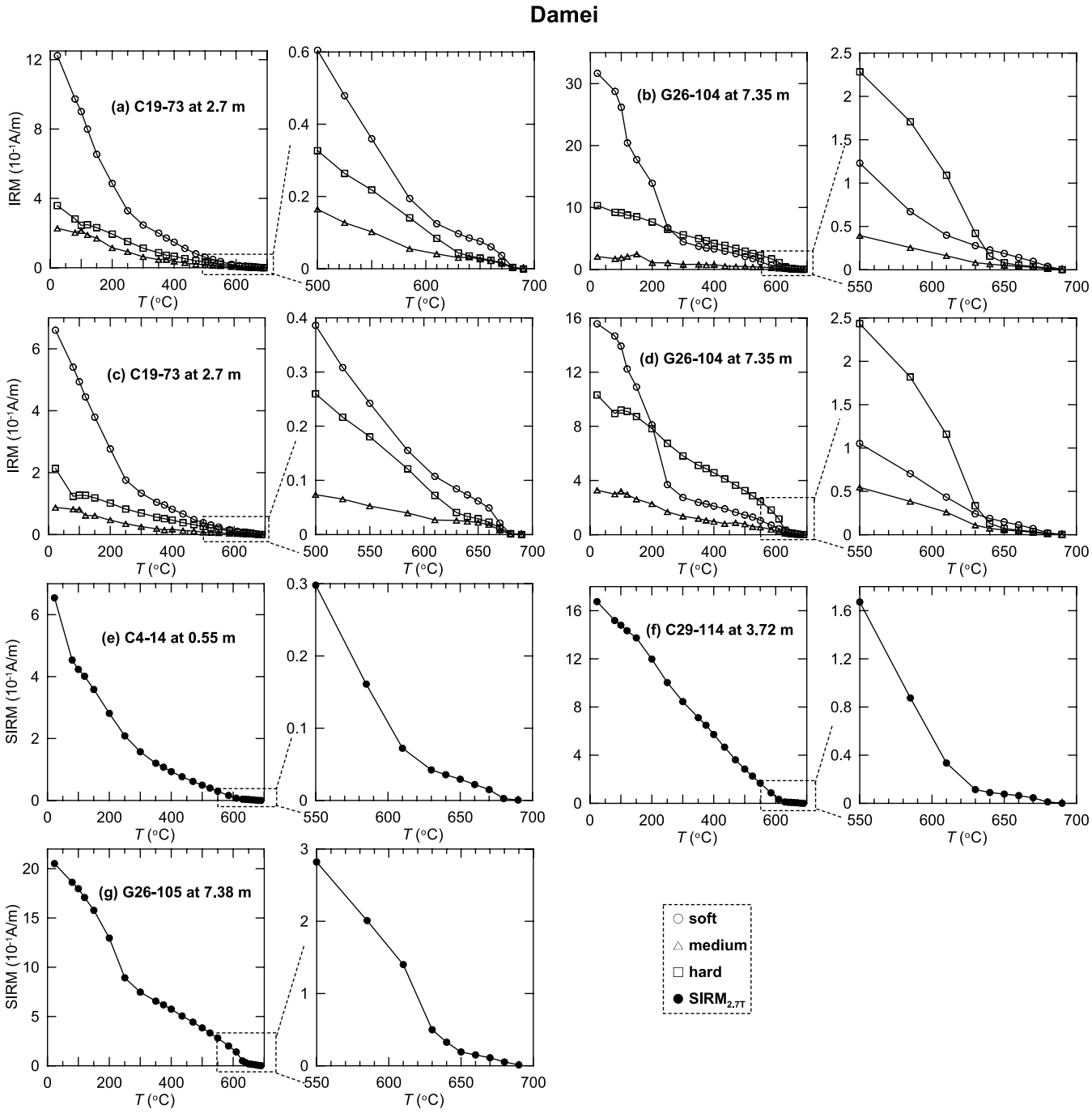

Figure 9. (a–b) Progressive thermal demagnetization of a three-component IRM (Lowrie 1990) produced by magnetizing samples from the Damei section in 2.7, 0.5 and 0.05 T along the *Z*-, *Y*- and *X*-axes, respectively. (c–d) Progressive thermal demagnetization of a three-component IRM (Lowrie 1990), which is produced by magnetizing samples of the Damei section in 2.7, 0.5 and 0.05 T along the *Z*-, *Y*- and *X*-axes, respectively, and then demagnetized in an alternating field of 60 mT along the *Z*-, *Y*- and *X*-axes. (e–g) Progressive thermal demagnetization of SIRM, which is produced by magnetizing samples of the Damei section in 2.7 T along the *Z*-axis and then demagnetized in an alternating field of 100 mT also along the *Z*-axis.

geomagnetic event due to the longer duration, which can make it easier to record than the other two events. In addition, two polarity flips, represented by anomalous VGPs from single samples, are labelled f1 and f2 in Fig. 12e. One flip within magnetozone N1 and the other within magnetozone R1, are observed in the Xuancheng sequence, which may be attributed to the artefacts of the remanence-recording process because these two flips appeared in the lithological unit of strong vermiculated red silty clay (Fig. 12a), which has experienced extremely warm and humid climate (Yin & Guo 2006; Yuan *et al.* 2008).

Considering the age of the Santa Rosa geomagnetic event, which has been dated at 0.91–0.94 Ma by $^{40}Ar/^{39}Ar$ age determination of volcanic rocks (Singer *et al.* 1999; Singer & Brown 2002), we evaluate that the Xuancheng red soil sequence started to accumulate at 0.9–1.0 Ma. Our constructed magnetostratigraphy of the Xuancheng section is consistent with that reported by Qiao *et al*.

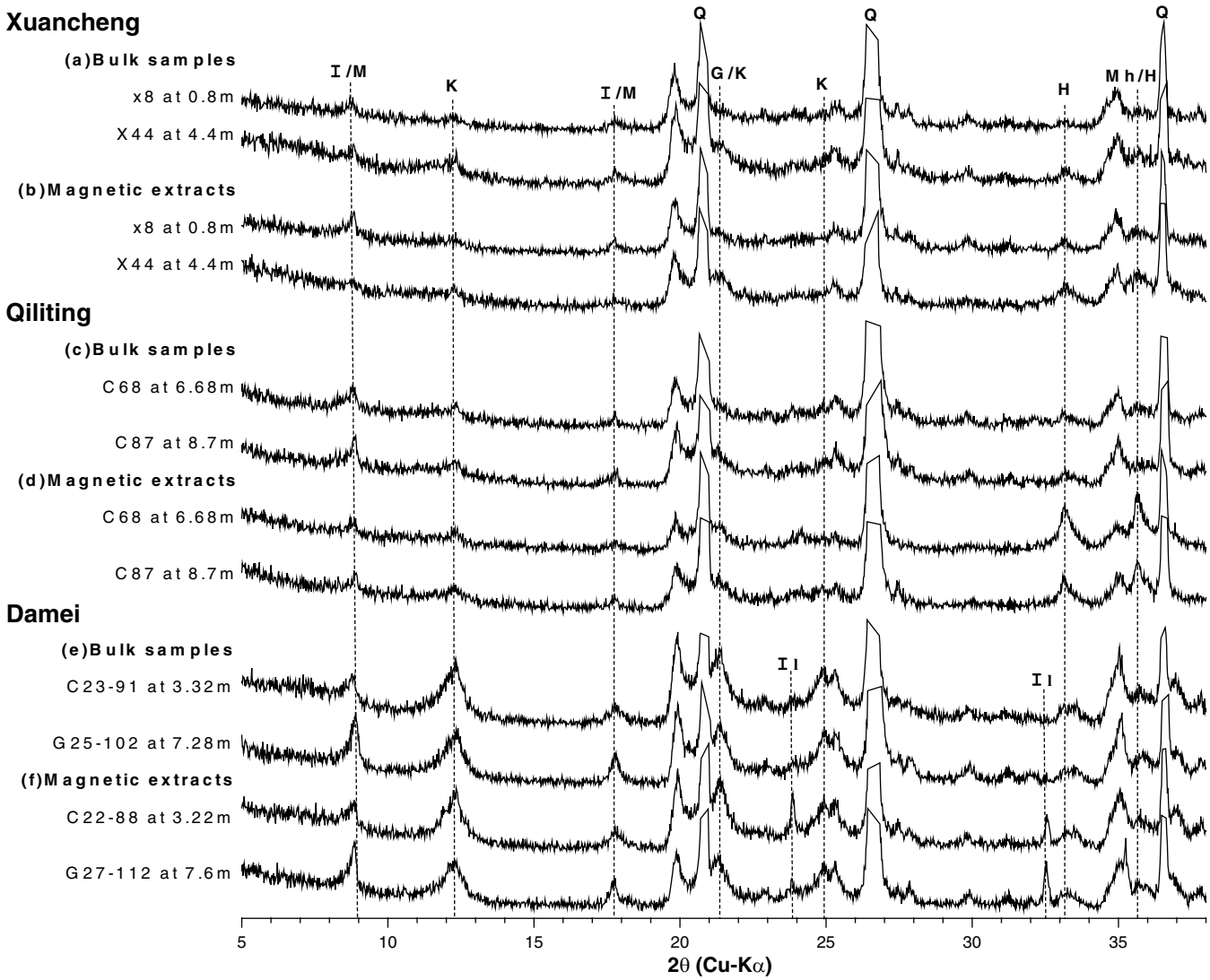

Figure 10. XRD spectra of bulk samples and magnetic extracts for selected samples from the Xuancheng (a and b), Qiliting (c and d) and Damei (e and f) sections. Data shown in (c and d) are after Liu *et al*. (2008). Data shown in (e) are after Deng *et al*. (2007). G, goethite; H, haematite; Mh, maghemite; K, kaolinite; I, illite; Il, ilmenite; M, muscovite; Q, quartz.

(2003). Our results reveal more fine structures of the late Matuyama reverse chron.

5 DISCUSSION

The wasp-waisted behaviour of hysteresis loops of red soil samples from our studied sequences (Fig. 5) indicates the coexistence of two magnetic mineral components with contrasting coercivities (Roberts *et al.* 1995). This can be further demonstrated by the rapid rise in the IRM acquisition curves below 300 mT (Fig. 4) (low-coercivity components) and the continuous increase in IRM above 300 mT (high-coercivity components), and the low values of S ratio (high-coercivity components).

For these three studied profiles, as suggested by the χ–T (Fig. 2) and M_s–T (Fig. 3) curves, and by the thermal demagnetization of the three-component IRM and $SIRM_{2.7T}$ (Figs 7–9), the low-coercivity magnetic mineral components are magnetite and maghemite. However, in the Damei red soil sequence, magnetite is present, but to a lesser extent, as indicated by the thermal demagnetization of the three-component IRM (Figs 9a and c). The high-coercivity magnetic minerals consist of haematite and goethite identified by the thermal demagnetization of the three-component IRM and $SIRM_{2.7T}$ (Figs 7–9). The presence of haematite was also confirmed by the χ–T curves (Fig. 2) and the XRD spectra (Fig. 10).

All of the magnetic minerals identified earlier contribute to the NRM, but only magnetite and haematite ($T_B = 680\ ^\circ C$) dominate the ChRM of the Xuancheng deposits, and only haematite ($T_B = 680\ ^\circ C$) dominates the ChRM of the Qiliting deposits. Although these magnetic minerals are of different origins, for example aeolian for the Xuancheng sequence and fluvial for the Qiliting sequence, they all belong to detrital products, which carry the primary detrital remanence. More interestingly, in the Damei red soil sequence, the haematite can be classified into two types: one with unblocking temperature of 680 °C and the other with unblocking temperature of 630–640 °C (Figs 2 and 9). The former should be of detrital origin, whereas the latter is pedogenic product.

In our previous study, only a normal magnetozone is recognized in the Damei sequence (Deng *et al.* 2007). This has been shown

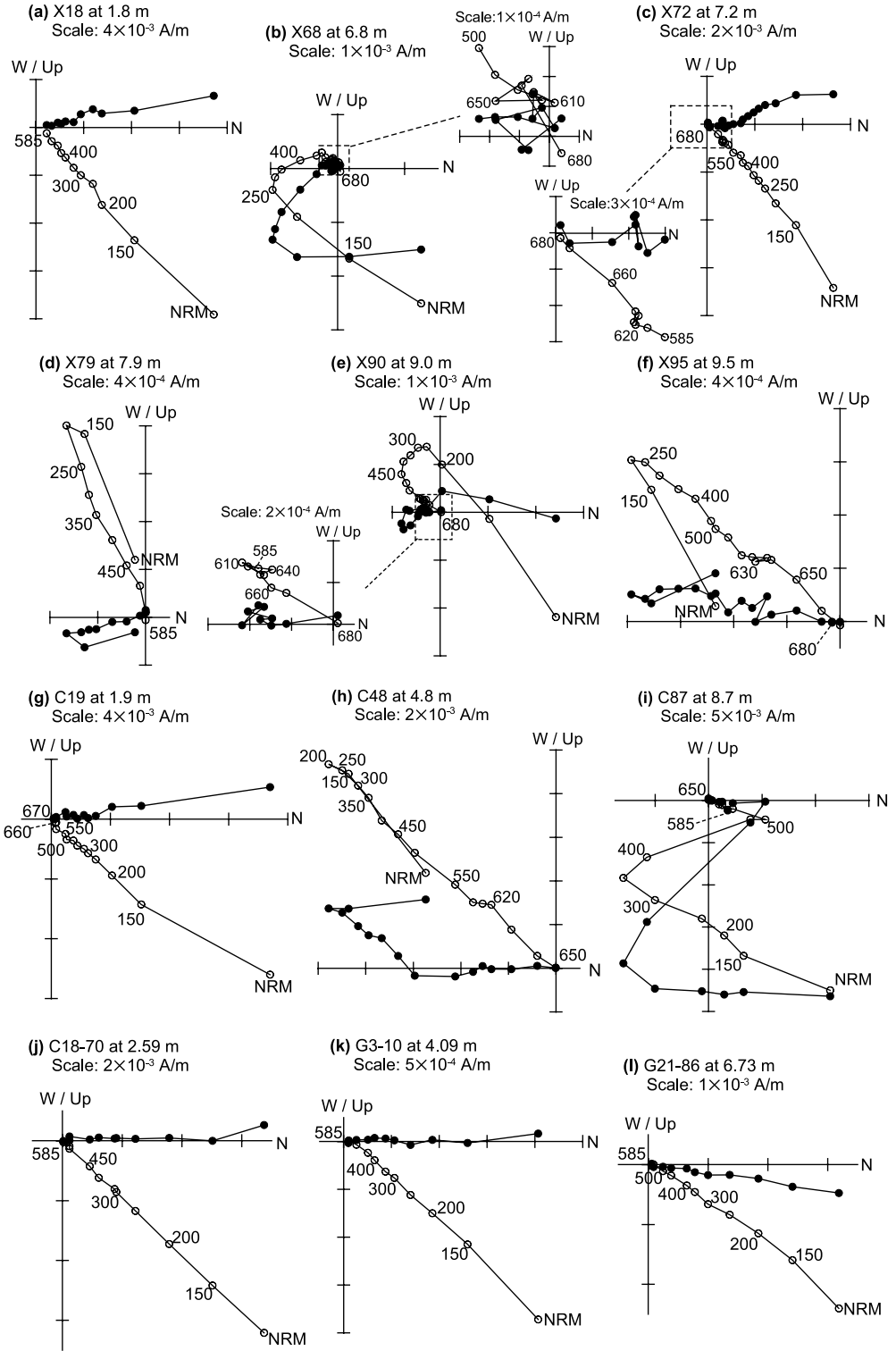

Figure 11. Orthogonal projections of representative progressive thermal demagnetization for selected samples from the Xuancheng (a–f), Qiliting (g–i) and Damei (j–l) sections. Data shown in (g–i) are after Liu *et al*. (2008). The solid (open) circles represent the horizontal (vertical) planes. The numbers refer to the temperatures in °C. NRM is the natural remanent magnetization.

to be a false recording of the geomagnetic field when considering the $^{40}Ar/^{39}Ar$ age of the tektites within the Bose Basin red soils, which have been dated to be 803 ka (Hou *et al.* 2000) and is just close to the Matuyama–Brunhes geomagnetic reversal (Fig. 12o). According to our rock magnetic results, goethite does not make a significant contribution to the NRM (Figs 6f and 11j–l). Furthermore, the remanence carried by goethite can be removed by thermal demagnetization to 150 °C, which means that it cannot be an overprint on the primary remanence. Pedogenic maghemite with T_B of 350 °C can be removed by thermal demagnetization to

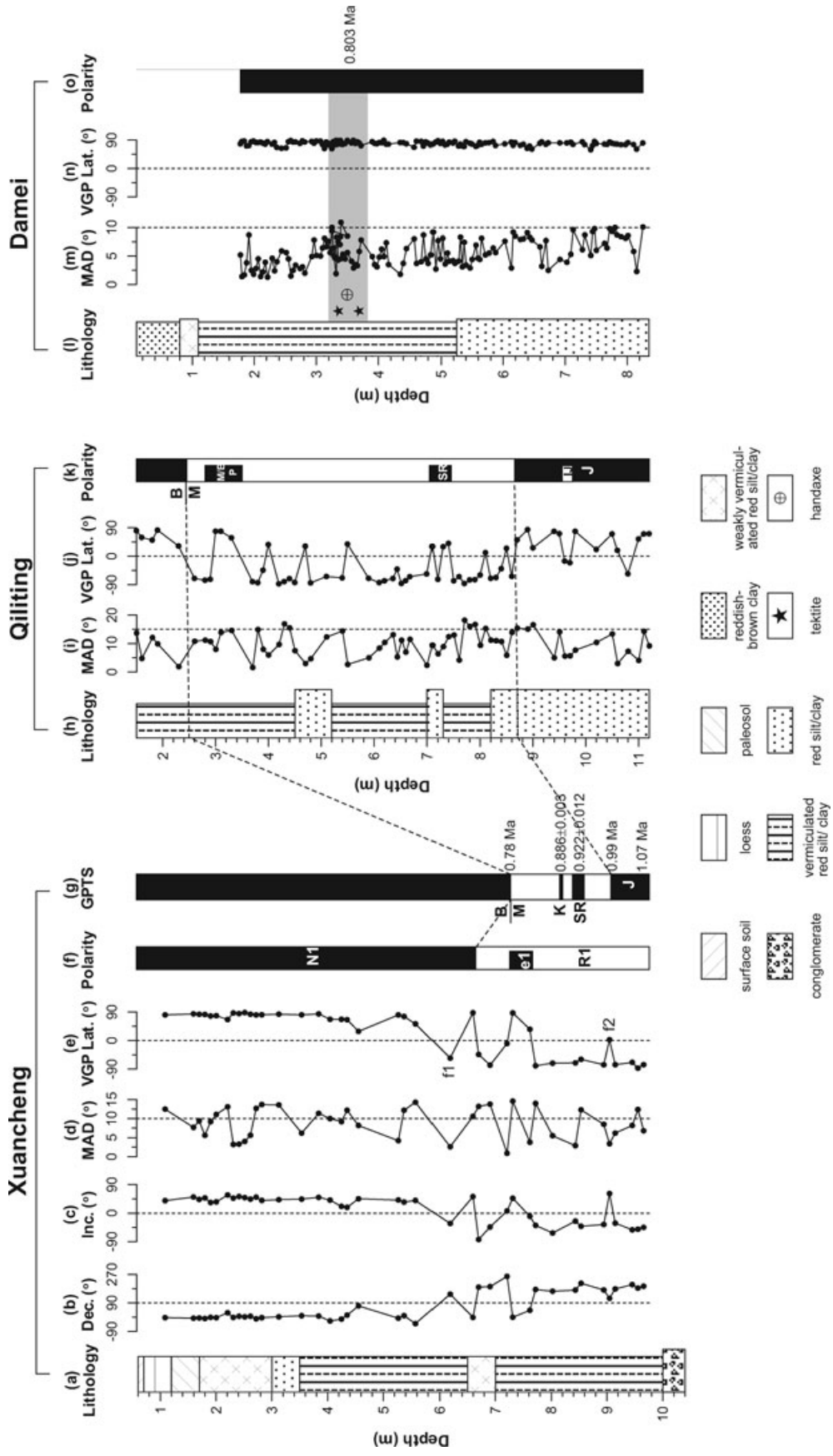

Figure 12. (a–g) Lithostratigraphy and magnetic polarity stratigraphy of the Xuancheng sequence and its correlation with the geomagnetic polarity timescale (GPTS) (Cande & Kent 1995; Singer *et al.* 1999, 2002; Lourens *et al.* 2004). f1 and f2 in (e) represent polarity flips. N1 and R1 in (f) represent magnetozones. e1 in (f) represent a short interval of possible transitional field behaviour. (h–k) Lithostratigraphy and magnetic polarity stratigraphy of the Qiliting sequence (after Liu *et al.* 2008). (l–o) Lithostratigraphy and magnetic polarity stratigraphy of the Damei sequence (after Deng *et al.* 2007). B, Brunhes; M, Matuyama; J, Jaramillo; K, Kamikatsura; SR, Santa Rosa; II, intra-Jaramillo; M/B P, Matuyama-Brunhes precursor; Dec., declination; Inc., inclination; MAD, maximum angular deviation; VGP Lat., latitude of the virtual geomagnetic pole.

350 °C. Magnetite is only present in small quantities, and is unlikely to significantly influence the palaeomagnetic results. The type of haematite with $T_B = 680$ °C may be of detrital origin, which may carry the primary remanence overprinted by a secondary remanence. The second type of haematite, with unblocking temperature of 630–640 °C, has high coercivity and remanent coercivity, which is confirmed by the thermal demagnetization curve of the hard fraction of the three-component IRM (Figs 9a–d), and the open nature of hysteresis loop up to 1 T (Fig. 5f). The relatively lower unblocking temperature compared to specular haematite is due to its fine grain size and Al-substitution, which have been shown to be the characteristics of secondary pedogenic pigment haematite (Tauxe *et al.* 1980). This pedogenic haematite has made significant contribution to natural remanence and overprinted the signal of detrital haematite (Figs 6e, 9 and 11j–l). Therefore, the overprinting on the primary remanence is attributed to the abundant presence of pedogenic haematite, which carries a CRM with high intensity.

Pedogenic haematite is the primary red pigment component in the Bose Basin. The red pigment is commonly present in warm subtropical and tropical areas, and forms after deposition, owing to *in situ* alteration of iron silicates and other iron-bearing detrital grains such as ilmenite and magnetite. According to Walker's (1967) summary, the iron oxide pigment in red soil has three main forms, which are related to both age and climatic intensity (Van Houten 1973): (1) brown amorphous ferric oxide—the dominant pigment in the younger soils or under mild climate condition; (2) red amorphous and poorly crystallized ferric oxide, which does not give a diagnostic XRD pattern, such as poorly crystallized haematite—this type, or combination of types of iron oxide are the dominant pigment in the older, redder soils and (3) red well-crystallized haematite, which may form during diagenesis. Among our studied sequences, the goethite and abundant pedogenic maghemite present in the Xuancheng and Qiliting sequences are related to the first-stage form, whereas the authigenic pigment haematite, which is too poorly crystallized to show the diagnostic XRD peak (Fig. 10), belongs to the second-stage pigment form. This pigment haematite controls the iron oxide pigment of the Damei sequence. The pedogenic maghemite and goethite, which coexist with the pigment haematite in the Damei sequence, also belong to the second-stage pigment form. This behaviour suggests that the two areas may be of different age or have experienced different weathering intensity. Previous studies have reached the consensus that the red soil sequences in southern China were formed from the late Early to Middle Pleistocene (e.g. Liu *et al*. 2008; Yuan *et al*. 2008). Moreover, the similarity of the lithostratigraphies of these three sequences also indicates that they have accumulated during the same period (Fig. 12). Therefore, the pigment components here are products controlled by the local weathering intensity and not age.

The Xuancheng and Qiliting sequences are both located in the lower reaches of the Yangtze River under the subtropical monsoon climatic condition with a MAT of 15–16 °C and a MAP of 1122–1400 mm (Qiao *et al.* 2003; Liu *et al.* 2008). Our results indicate that such a warm–wet subtropical climate can induce a moderate degree of chemical weathering, and thus only produce the first-stage brown ferric oxide pigment—the pedogenic maghemite and goethite, whose contributions were not strong enough to overprint the signals of the primary detrital magnetic minerals. In other words, the alteration of the detrital magnetic grains to the ferric oxide pigment is so little that most of the primary signals can be preserved.

The region of the Damei section, Bose basin, has a MAT of ∼22 °C and a MAP of ∼1100 mm. The precipitation is not evenly distributed throughout the year, but has a prominent dry season from October to March and wet season from June to August (Deng *et al.* 2007). Higher concentrations of kaolinite suggest a strong weathering (Fig. 10). This strong weathering may be correlative with elevated temperature. The seasonal dry–wet alternation, coupled with higher MAT and relatively lower MAP in the Bose Basin may have greatly accelerated the conversion of brown ferric oxides (e.g. maghemite and goethite) to red haematite pigment (Lu *et al.* 2008), which resulted in the formation of abundant pedogenic haematite, as suggested by the low *S*-ratio values (Fig. 4) and the thermal demagnetization of the three-component IRM and $SIRM_{2.7T}$ (Fig. 9). This type of pedogenic haematite may be present in large enough quantities to overprint the primary remanence, or most of the detrital ferric grains have been sufficiently altered to the red pigment, which destroyed the primary detrital remanence.

It is therefore concluded that climate conditions have a significant influence on the palaeomagnetic records and it needs to be taken into consideration when dealing with the magnetostratigraphic results from intensely warm–humid, especially seasonally humid, climate regions. Furthermore, the red pigment component, such as pedogenic haematite, which suggests intensified postdepositional chemical weathering, may be used as an indicator for the degree of remagnetization in red soil sequences.

6 CONCLUSIONS

We have analysed detailed mineral magnetic, petrographic and/or palaeomagnetic records from three red soil sequences in southern China: the Xuancheng and Qiliting sequences located in the lower reaches of the Yangtze River and the Damei sequence in the Bose Basin. Palaeomagnetic results show that the Xuancheng sequence has recorded the Brunhes chron and the late Matuyama chron, including a short interval probably representing the Santa Rosa geomagnetic event. The Xuancheng and Qiliting sequences have faithfully recorded the palaeogeomagnetic field whereas the Damei sequence failed. All the three sections have two magnetic components of high- and low-coercivity. Maghemite, magnetite, goethite and haematite are all contained in the studied three red soil sequences. The ChRM carriers are magnetite and haematite ($T_B = 680$ °C) in the Xuancheng sequence, only haematite ($T_B = 680$ °C) in the Qiliting sequence, and pedogenic haematite with T_B of about 630–640 °C in the Damei sequence. Comparing the magnetic mineral assemblages of these three sections, we find that the pedogenic haematite with T_B of about 630–640 °C carries abundant CRM, which overprints the NRM of the Damei red soils. The formation of this pedogenic haematite with high coercivity is mainly controlled by chemical weathering which was greatly intensified by the climate of high MAT, relatively lower MAP and the stronger seasonal dry–wet alternation in the region of the Damei sequence. We infer that in some cases climatic conditions control the reliability of palaeomagnetic results and the red pigment components may be used as an indicator for the degree of remagnetization.

ACKNOWLEDGMENTS

We are grateful to the Editor, Professor Erwin Apple and to Drs. Christoph Geiss and Greig Paterson for their insightful comments and suggestions, which have significantly improved the paper. Palaeomagnetic and mineral magnetic measurements were made in the Palaeomagnetism and Geochronology Laboratory (SKL-LE), Institute of Geology and Geophysics, Chinese Academy of Sciences.

Financial assistance was provided by the National Natural Science Foundation of China (grants 40925012 and 40821091), the Ministry of Science and Technology of China (grant 2007FY110200) and the Chinese Academy of Sciences. Q. Liu acknowledges further support from the 100-talent Program of the Chinese Academy of Sciences.

REFERENCES

Cande, S.C. & Kent, D.V., 1995. Revised calibration of the geomagnetic polarity timescale for the Late Cretaceous and Cenozoic, *J. geophys. Res.,* **100**(B4), 6093–6096.

Channell, J.E.T., Mazaud, A., Sullivan, P., Turner, S. & Raymo, M.E., 2002. Geomagnetic excursions and paleointensities in the Matuyama Chron at Ocean Drilling Program Sites 983 and 984 (Iceland Basin), *J. geophys. Res.,* **107**(B6), doi:10.1029/2001JB000491.

Chen, J. & Wang, H.N., 2004. *Geochemistry: Geochemistry of Weathering,* p. 418, Science Press, Beijing.

Coe, R.S., Singer, B.S., Pringle, M.S. & Zhao, X.X., 2004. Matuyama-Brunhes reversal and Kamikatsura event on Maui: palaeomagnetic directions $^{40}Ar/^{39}Ar$ ages and implications, *Earth planet. Sci. Lett.,* **222,** 667–684.

Deng, C.L., Zhu, R.X., Jackson, M.J., Verosub, K.L. & Singer, M.J., 2001. Variability of the temperature-dependent susceptibility of the Holocene eolian deposits in the Chinese loess plateau: a pedogenesis indicator, *Phys. Chem. Earth (A)*, **26**(11–12), 873–878.

Deng, C.L., Wei, Q., Zhu, R.X., Wang, H.Q., Zhang, R., Ao, H., Chang, L. & Pan, Y.X., 2006. Magnetostratigraphic age of the Xiantai Paleolithic site in the Nihewan Basin and implications for early human colonization of Northeast Asia, *Earth planet. Sci. Lett.,* **244,** 336–348.

Deng, C.L., Liu, Q.S., Wang, W. & Liu, C.C., 2007. Chemical overprint on the natural remanent magnetization of a subtropical red soil sequence in the Bose Basin, southern China, *Geophys. Res. Lett.,* **34,** L22308, doi:10.1029/2007GL031400.

Dunlop, D.J. & Özdemir, Ö., 1997. *Rock Magnetism: Fundamentals and Frontiers,* p. 573, Cambridge University Press, Cambridge, UK.

Fang, Y.S., 1997. A report on excavation of Chenshan locality in 1988, Anhui province, *Acta Anthropol. Sin.,* **16**(2), 96–106.

Hart, P. & Tauxe, L., 1996. A precursor to the Matuyama/Brunhes transition-field instability as recorded in pelagic sediments, *Earth planet. Sci. Lett.,* **138,** 121–135.

Herbillon, A.J. & Nahon, D., 1988. Laterites and lateritization processes, in *Iron in Soils and Clay Minerals,* pp. 779–796, eds. Stucki, J.W., Goodman, B.A. & Schwertmann, U., Reidel D., Dordrecht, Netherlands.

Horng, C.S., Roberts, A.P. & Liang, W.T., 2003. A 2.14-Myr astronomically tuned record of relative geomagnetic paleointensity from the western Philippine Sea, *J. geophys. Res.*, **108**(B1), 2059, doi:10.1029/2001JB001698.

Hou, Y.M., Potts, R., Yuan, B.Y., Guo, Z.T., Deino, A., Wang, W., Clark, J., Xie, G.M. *et al*., 2000. Mid-Pleistocene Acheulean-like stone technology of the Bose Basin, South China, *Science,* **287,** 1622–1626.

Hunt, C.P., Banerjee, S.K., Han, J., Solheid, P.A., Oches, E., Sun, W. & Liu, T., 1995. Rock-magnetic proxies of climate change in the loess-paleosol sequences of the western Loess Plateau of China, *Geophys. J. Int.,* **123,** 232–244, doi:10.1111/j.1365-246X.1995.tb06672.x.

Jiang, F.C., Wu, X.H., Xiao, H.G., Zhao, Z.Z., Wang, S.M. & Xue, B., 1997. Age of the vermiculated red soil in Jiujiang area, central China (in Chinese with English abstract), *J. Geomech.,* **3**(4), 27–32.

King, J.W. & Channell, J.E.T., 1991. Sedimentary magnetism, environmental magnetism, and magnetostratigraphy, *U.S. Natl. Rep. Int. Union Geod. geophys. 1987–1990, Rev. geophys.,* **29,** 358–370.

Kirschvink, J.L., 1980. The least-squares line and plane and the analysis of palaeomagnetic data, *Geophys. J. R. astr. Soc.,* **62,** 699–718.

Laj, C. & Channell, J.E.T., 2007. Geomagnetic excursions, in *Treatise on Geophysics,* Vol. **5**: Geomagnetism, Encyclopedia of Geophysics, pp. 373–416, ed. Kono, M., Elsevier, Amsterdam.

Liu, Q.S., Torrent, J., Yu, Y.J. & Deng, C.L., 2004. Mechanism of the parasitic remanence of aluminous goethite [α-(Fe, Al)OOH], *J. geophys. Res.,* **110,** B12106, doi:10.1029/2004JB003352.

Liu, Q.S., Deng, C.L., Yu, Y.J., Torrent, J., Jackson, M.J., Banerjee, S.K. & Zhu, R.X., 2005. Temperature dependence of magnetic susceptibility in argon environment: Implications for pedogenesis of Chinese loess/palaeosols, *Geophys. J. Int.,* **161,** 102–112.

Liu, C.C., Xu, X.M., Yuan, B.Y. & Deng, C.L., 2008. Magnetostratigraphy of the Qiliting section (SE China) and its implication for geochronology of the red soil sequences in southern China. *Geophys. J. Int.,* **174,** 107–114.

Lourens, L., Hilgen, F., Shackleton, N.J., Laskar, J. & Wilson, D., 2004. The Neogene Period, in *A Geologic Time Scale,* pp. 409–440, eds Gradstein, F.M., Ogg, J.G. & Smith, A.G., Cambridge University Press, Cambridge, UK.

Lowrie, W., 1990. Identification of ferromagnetic minerals in a rock by coercivity and unblocking temperature properties, *Geophys. Res. Lett.,* **17**(2), 159–162.

Lu, S.G., 2000. Lithological factors affecting magnetic susceptibility of subtropical soils, Zhejiang Province, China, *Catena,* **40,** 359–373.

Lu, S.G., 2007. Environmental magnetism of Quaternary red earth in southern China (in Chinese with English abstract), *Quat. Sci.,* **27,** 1016–1022.

Lu, S.G., Xue, Q.F., Zhu, L. & Yu, J.Y., 2008. Mineral magnetic properties of a weathering sequence of soils derived from basalt in Eastern China, *Catena,* **73,** 23–33.

Oches, E.A. & Banerjee, S.K., 1996. Rock-magnetic proxies of climate change from loess-paleosol sediments of the Czech Republic, *Studia geoph. et geod.,* **40**, 287–300.

Opdyke, N.D. & Channell, J.E.T., 1996. *Magnetic Stratigraphy,* p. 346, Academic Press, San Diego, CA.

Özdemir, Ö. & Banerjee, S.K., 1984. High temperature stability of maghemite (γ–Fe_2O_3), *Geophys. Res. Lett.,* **11**(3), 161–164.

Potts, R., 2001. Mid-Pleistocene environmental change and human evolution, in *Human Roots: Africa and Asia in the Middle Pleistocene,* pp. 5–21, eds Barham, L. & Robson-Brown, K., Western Academic and Specialist Press Limited, Bristol.

Potts, R., Huang, W.W., Hou, Y.M., Deino, A., Yuan, B.Y., Guo, Z.T. & Clark, J., 2000. Reply to 'Tektites and the age paradox in mid-Pleistocene China', *Science,* **289,** 507a.

Qiao, Y.S. *et al*., 2003. Loess-soil sequence in southern Anhui Province: magnetostratigraphy and paleoclimatic significance, *Chinese Sci. Bull.,* **48,** 2088–2093.

Roberts, A.P., Cui, Y. & Verosub, K.L., 1995. Wasp-waisted hysteresis loops: mineral magnetic characteristics and discrimination of components in mixed magnetic systems, *J. geophys. Res.,* **100,** 17 909−17 924.

Shive, P.N. & Diehl, J.F., 1977. Reduction of haematite to magnetite under natural and laboratory conditions, *Adv. Earth. Planet. Sci.,* **1,** 113–122.

Singer, B.S. & Brown, L.L., 2002. The Santa Rosa Event: $^{40}Ar/^{39}Ar$ and paleomagnetic results from the Valles rhyolite near Jaramillo Creek, Jemez Mountains, New Mexico, *Earth planet. Sci. Lett.,* **197,** 51–64.

Singer, B.S., Hoffman, K.A., Chauvin, A., Coe, R.S. & Pringle, M.S., 1999. Dating transitionally magnetized lavas of the late Matuyama Chron: toward a new $^{40}Ar/^{39}Ar$ timescale of reversals and events, *J. geophys. Res.,* **104,** 679–693.

Singer, B.S., Relle, M.K., Hoffman, K.A., Battle, A., Laj, C., Guillou, H. & Carracedo, J.C., 2002. Ar/Ar ages from transitionally magnetized lavas on La Palma, Canary Islands, and the geomagnetic instability timescale, *J. geophys. Res.,* **107**(B11), 2307, doi:10.1029/2001JB001613.

Stacey, F.D. & Banerjee, S.K., 1974. *The Physical Principles of Rock Magnetism,* p. 195, Elsevier, Amsterdam.

Tauxe, L., Kent, D.V. & Opdyke, N.D., 1980. Magnetic components contributing to the NRM of middle siwalik red beds, *Earth planet. Sci. Lett.,* **47,** 279–284.

Teilhard de Chardin, P., Young, C.C., Pei, W.C. & Chang, H.C., 1935. On the Cenozoic formations of Kwangsi and Kwangtung, *Bull. geol. Soc. China,* **14,** 181–205.

Van Houten, F.B., 1973. Origin of Red Beds a review—1961–1972, *Annu. Rev. Earth planet. Sci.,* **1,** 39–61.

Verosub, K.L. & Roberts, A.P., 1995. Environmental magnetism: past, present, and future, *J. geophys. Res.,* **100,** 2175–2192.

Walker, T.R., 1967. Formation of Red Beds in modern and ancient deserts, *Geol. Soc. Am. Bull.,* **78,** 353–368.

Wang, H.Q., Deng, C.L., Zhu, R.X., Wei, Q., Hou, Y.M. & Boëda, E., 2005. Magnetostratigraphic dating of the Donggutuo and Maliang Paleolithic sites in the Nihewan Basin, North China, *Quat. Res.,* **64,** 1–11.

Wang, W., Mo, J.Y. & Huang, Z.T., 2008. Recent discovery of handaxes associated with tektites in the Nanbanshan locality of the Damei site, Bose basin, Guangxi, South China, *Chin. Sci. Bull.,* **53**(6), 878–883.

Xi, C.F., 1991. On the red weathering crusts of southern China (in Chinese with English abstract), *Quat. Sci.,* **1,** 1–8.

Xu, X.M., 2007. Paleolithic artifacts found in Changxing County, Zhejiang Province, *Acta Anthropol. Sin.,* **26**(1), 16–25.

Xiong, S.F., Sun, D.H. & Ding, Z.L., 2002. Aeolian origin of the red earth in southeast China, *J. Quat. Sci.,* **17,** 181–191.

Yang, X.Q., Zhu, Z.Y., Zhang, Y.N., Li, H.M., Zhou, W.J. & Yang, J., 2008. Rock magnetic properties and palaeomagnetic results of sediments from a stone implement layer in the Bose Basin, Guangxi, *Sci. China, Ser. D,* **51,** 441–450.

Yin, Q.Z. & Guo, Z.T., 2006. Mid-Pleistocene vermiculated red soils in southern China as an indication of unusually strengthened East Asian monsoon, *Chin. Sci. Bull.,* **51,** 213–220.

Yong, C.C., Bien, M.N. & Lee, Y.Y., 1938. 'Red Beds' of Hunan, *Bull. Geol. Soc. China,* **18** (3–4), 259–300.

Yuan, B.Y. *et al*., 2008. Chronostratigraphy and stratigraphic division of red soil in southern China (in Chinese with English abstract), *Quat. Sci.,* **28,** 1–13.

Zhao, Q.G. & Yang, H., 1995. A preliminary study of red earth and changes of Quaternary environment in South China (in Chinese with English abstract), *Quat. Sci.,* **2,** 107–115.

Zhao, Z.Z., Qiao, Y.S., Wang, Y., Fu, J.L., Wang, S.B., Li, C.Z., Yao, H.T. & Jiang, F.C., 2007. Magnetostratigraphic and paleoclimatic studies on the Red Earth Formation from the Chengdu Plain in Sichuan Province, China, *Sci. China, Ser. D,* **50,** 927–935.

Zhu, R.X., Zhou, L.P., Laj, C., Mazaud, A. & Ding, Z.L., 1994. The Blake geomagnetic polarity episode recorded in Chinese loess, *Geophys. Res. Lett.,* **21**(8), 697–700.

Zijderveld, J.D.A., 1967. A.C. demagnetization of rocks: analysis of results, in *Methods in Paleomagnetism,* pp. 254–286, eds. Collinson, D.W., Creer, K.M., & Runcorn, S.K., Elsevier, New York.